Journal of Non-Crystalline Solids 378 (2013) 115–120

Crystal nucleation and growth kinetics of NaF in photo-thermo-refractive glass

I. Dyamant [a], A.S. Abyzov [b], V.M. Fokin [c,*], E.D. Zanotto [a], J. Lumeau [e], L.N. Glebova [d], L.B. Glebov [d]

[a] Vitreous Materials Laboratory, Department of Materials Engineering, Federal University of São Carlos, UFSCar, 13565-905 São Carlos, SP, Brazil
[b] National Science Centre Kharkov Institute of Physics and Technology, Ukraine
[c] Vavilov State Optical Institute, ul. Babushkina 36-1, 193 171 St. Petersburg, Russia
[d] CREOL, The College of Optics and Photonics, University of Central Florida, PO Box 162700, Orlando, FL 32816-2700, United States
[e] Aix-Marseille Université, CNRS, Centrale Marseille, Institut Fresnel, UMR 7249, 13013, France

ARTICLE INFO

Article history:
Received 29 April 2013
Received in revised form 22 June 2013
Available online 19 July 2013

Keywords:
PTR glass;
Nucleation;
Time-lag;
Crystal growth;
Crystallization

ABSTRACT

Photo-thermo-refractive (PTR) glass is an optically transparent photosensitive oxide glass. Upon heating, the UV-exposed regions of this glass undergo copious crystallization of NaF nano-crystals giving rise to a permanent, localized refractive index change. But the unexposed parts of the glass also undergo some crystallization which causes unwanted light scattering. Holographic optical elements produced from PTR glass have been used in special laser systems. In this article we report, for the first time since the invention of PTR glass about half a century ago, the steady-state nucleation rates, nucleation time-lags and crystal growth rates for UV-unexposed PTR glass estimated in a wide temperature range, from T_g ~ 470 °C up to 750 °C. A self-consistent description of these data is presented in the framework of classical nucleation theory using the interfacial free energy of the critical nuclei and the effective diffusion coefficient as adjustable parameters. The diffusivity calculated from crystallization kinetics and that estimated from viscous flow via the Stokes–Einstein–Eyring equation show a decoupling phenomenon.

1. Introduction

Photo-thermo-refractive (PTR) glass is a Si–Na–Al–Zn–Br–F oxide glass doped with Ce, Ag, Sb and Sn. Upon heating, the UV-exposed regions of this photosensitive glass undergo copious crystallization of NaF nano-crystals, giving rise to a permanent, localized refractive index change. Holographic optical elements produced from this optically transparent glass have been increasingly used in special laser systems.

Unfortunately, the un-exposed regions of PTR glass also undergo crystallization upon adequate heat treatment, but the number of crystals is larger in the UV-exposed regions [1]. The significance of knowing the detailed crystal nucleation and growth kinetics in both UV-exposed and un-exposed PTR glass stems from the fact that these kinetic parameters help to design proper thermal treatments to reach the wanted degree of crystallinity and crystal size distribution in order to achieve the desired optical effect (localized, permanent refractive index change) and, at the same time, to optimize optical transmission and to minimize light scattering.

The study of the crystallization kinetics of NaF in PTR glass has not only practical but also theoretical importance, since PTR glass provides a good model for analyzing processes of nucleation and growth of a minor phase, in this case sodium fluoride, i.e. when a strong difference between the compositions of the parent glass and the precipitated crystalline phase takes place. In this case (at least in the advanced stages of the phase transformation) crystal growth is accompanied by the formation of diffusion zones that are depleted in fluoride and sodium and changes in the composition of the residual liquid [2]. The thermodynamic driving force for such type of crystallization is the supersaturation of the melt with respect to the dissolved phase, which, in this case, is crystalline NaF. At any given temperature, the thermodynamic driving force changes with time during crystallization becoming null when the NaF crystal volume fraction approaches the equilibrium value. By estimating the equilibrium volume fraction of NaF crystals, its solubility in PTR glass was estimated as a function of temperature [3]. It was shown in Ref. [4] that the presence of KBr reduces the solubility of the NaF crystals. This finding has clarified the role of bromine on the NaF crystallization in PTR glass. Moreover, liquid–liquid phase separation in PTR glass was first investigated and reported in Ref. [5].

Over 100 papers have been published worldwide with the keywords "photo thermo refractive glass" since 1999. The present paper is a logical continuation of these and our own long-standing systematic investigations intended to unveil the intricate *crystallization* process of PTR glass. In addition to the effects analyzed by us and briefly mentioned above [2–5], in Ref. [1] we have also studied already the overall crystallization kinetics of PTR glass by DSC methods. The present research is

* Corresponding author. Tel.: +7 812 695 30 38.
E-mail address: vmfokin@gmail.com (V.M. Fokin).

0022-3093/$ – see front matter © 2013 Elsevier B.V. All rights reserved.
http://dx.doi.org/10.1016/j.jnoncrysol.2013.06.027

aimed at the (difficult to perform) *direct measurement* of nucleation rates, time-lags and growth rates of NaF crystals in UV-un-exposed PTR glass as a function of temperature, and their analysis in the framework of classical nucleation theory (CNT).

2. Material and methods

A classical PTR glass with the composition $15Na_2O–5ZnO–4Al_2O_3–70SiO_2–5NaF–1KBr–0.01Ag_2O–0.01CeO–0.01SnO_2–0.03Sb_2O_3$ (mol%) was melted at 1460 °C in a platinum crucible, in air, and stirred for 5 h. Annealing was carried out at 460 °C for 1 h followed by cooling to room temperature at 0.1 K/min. Thus the resulting glass had already an extensive low temperature pre-history. We investigated the crystallization kinetics at higher temperatures beginning with the glass transition temperature $T_g = 470$ °C up to $T = 750$ °C.

The nucleation rate, I, is generally defined as

$$I = dN_V/dt, \tag{1}$$

where N_V is the number of supercritical crystals per unit volume and t is the time of nucleation. Hence, to estimate the nucleation rate at any given temperature one needs to know N_V as a function of nucleation time. The main problem in the experimental determination of I is, as a rule, the extremely small size of the crystals (only a few tens of Angstroms) nucleated and grown at any nucleation temperature, T_n. In order to reach a detectable nucleation rate, the undercoolings have to be sufficiently high. Due to the increase of the viscosity or the decrease of the effective diffusion coefficients with decreasing temperature, the crystal growth rates $U(T_n)$ at nucleation temperatures are often too small to allow the crystallites to grow to measurable sizes in reasonable experimental time scales. To overcome this problem we used the so called "development" method, proposed more than a hundred years ago by G. Tammann [6]. This method is frequently employed in nucleation studies. According to this technique, the crystals nucleated at T_n are grown at a higher temperature $T_d > T_n$ up to a size detectable in a light or electron microscope. The development temperature, T_d, has to satisfy the following conditions:

$$U(T_d) \gg U(T_n), \quad I(T_d) \ll I(T_n). \tag{2}$$

It should be noted (cf. also [7]), however, that not all crystals formed at T_n can develop at T_d, but only those grown at T_n up to a size larger than the critical size, R_d^*, corresponding to the critical cluster size at the development temperature, $T_d > T_n$. Recall that the critical size increases with temperature as we will show below. One can find more details about the "development" method in Refs. [7,8].

A very special problem in the analysis of nucleation rates in the case of PTR glass is the determination of the crystal number density, N_V. The dendritic shape of the crystals at T_d, and the very high values of N_V of the PTR glass samples strongly complicate the application of the standard stereological methods. Therefore, here we elaborated and used an approximate, fast, little material demanding method that gives reasonable, reproducible results. Small (100–500 μm) bits were prepared from heat-treated glass samples (chipped directly onto a transparent glass slide). Then the average distances, L, between the crystal centers were estimated using transmitted or reflected light microscopy. It should be noted that in the case of transmitted light, due to the small depth of field, most of the observed crystals were located within a very thin layer of the sample. The following approximate equation relates L with the average crystal number density N_V,

$$N_V = L^{-3}. \tag{3}$$

This equation could be employed to any system when N_V is large enough and the crystal shape cannot be approximated by a simple regular form (cube, sphere, ellipsoid or needle) to estimate the crystal number density with the proper equations.

The crystal growth rates were estimated by the standard procedure via crystal size vs. time plots.

3. Experimental results

A typical N_V^d versus nucleation time plot for the system under consideration is shown in Fig. 1. The superscript d denotes that this number density was obtained by the "development" method. The unusual (as compared with classical cases), non-monotonic growth of the $N_V^d(t)$-curve will be discussed later. Fig. 2 shows an example of NaF crystals grown at a relatively high temperature close to that employed for crystal development. Dendrite-like crystals have an approximately spherical external form, which we characterized by its maximal size ($2R$). Fig. 3 shows one of the plots of crystal size R ("radius") versus growth time. To estimate the crystal growth rate $U = dR/dt$ we used only the initial part of the $R(t)$-plot. The decrease of U during the advanced stage of phase transition will be commented later in the Discussion.

The values of $U(T)$ measured by the above described method are collected in Table 1 and plotted in Fig. 4 for different temperatures.

4. Treatment of the experimental data

As was noted in Section 2 not all crystals nucleated at T_n can be grown to detectable sizes at $T_d > T_n$ due to the following considerations. The critical crystal size is given by Eq. (4)

$$R^* = \frac{2\sigma}{\Delta G_V}. \tag{4}$$

Here σ (J/m^2) is the specific energy of the melt/critical crystal interface and ΔG_V (J/m^3) is the thermodynamic driving force for crystallization. The critical crystal size increases with temperature, mainly due to the decrease of ΔG_V. Hence all the crystals having sizes between the critical sizes R_n^* and R_d^*, corresponding to nucleation and "development" temperatures, respectively, dissolve at T_d. This dissolution effect results in a shift of the $N_V^d(T_n, T_d) \sim t$ curve estimated by the "development" method relative to the $N_V(T_n) \sim t$ curve, by a time t_o needed for the increase of cluster size from R_n^* to R_d^*, in such a way that

$$N_V(T_n, t) = N_V^d(T_n, (t - t_o)). \tag{5}$$

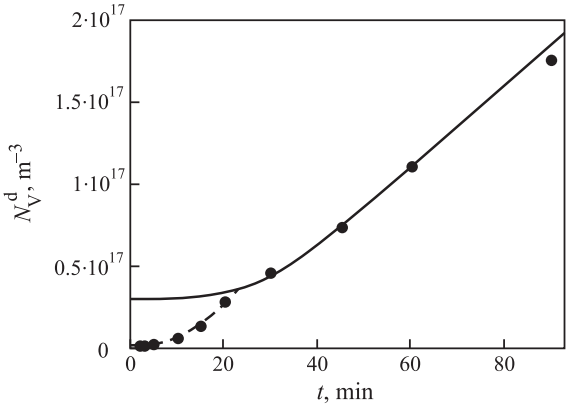

Fig. 1. Number density of NaF crystals developed at $T_d = 650$ °C versus time of nucleation treatment at $T_n = 530$ °C. The lines are plotted by Eq. (6).

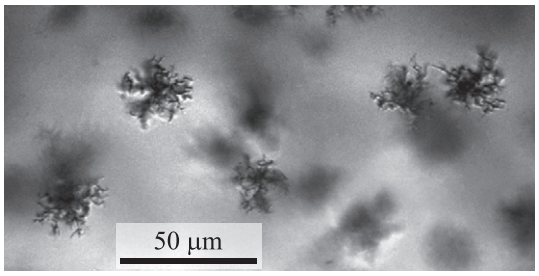

Fig. 2. Transmitted light optical micrographs of PTR glass samples treated at 690 °C for 25 min.

One can find more details about the development method in Refs. [8–11]. Thus, the crystals of the above described size interval must grow at T_n up to a size $R > R_d^*$ to be developed at T_d.

Two groups of crystals can be distinguished with respect to their formation conditions. The *first* group includes the crystals that have been nucleated at a given temperature T_n, i.e. reached the super critical size ($R > R_n^*$) during a time interval ($0 - t$) in the sequential random chain of attachment and detachment of the "structural" units to clusters of the new evolving phase (see e.g. [12]). In the (theoretical) case when the glass is obtained via an infinitely fast quenching of the melt after having performed a complete homogenization of the initial melt, one could assume that, in the first moments of nucleation heat-treatment at T_n, in the glass there are no clusters of subcritical size. In such case and if the cluster growth proceeds via the above described scheme, the nucleation process in such ideal system begins with the merging of two "structural" units. For the above initial condition, when the cluster size distribution is zero for all clusters containing more than a few structural units, the following expression describes the time-dependence of the number of super-critical nuclei per unit volume, N_V [13],

$$N_V(t) = I_{st}\tau\left(\frac{t}{\tau} - \frac{\pi^2}{6} - 2\sum_{m=1}^{\infty}\frac{(-1)^m}{m^2}\exp\left(-m^2\frac{t}{\tau}\right)\right), \quad (6)$$

where I_{st} is the steady-state nucleation rate, and τ the nucleation time-lag. Here τ characterizes the time of establishment of the steady-state crystal size distribution in a cluster size range including the critical size, and, hence, simultaneously the establishment in this range of cluster sizes of the steady-state value of the nucleation rate.

However, with the cooling rates usually employed for oxide glass preparation (1–1000 K/min) the initial glass samples already contain – due to cluster formation and growth in the course of the cooling process – a certain amount of crystals, N_o, having sizes R larger than the critical size R_n^* corresponding to the nucleation temperature T_n. These pre-existing crystals formed during melt cooling compose the

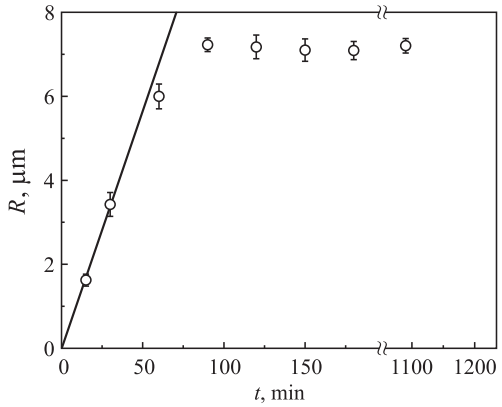

Fig. 3. Radius of NaF dendrite versus treatment time at $T = 650$ °C.

Table 1
Crystal growth rate versus temperature.

T, °C	U, m/s	Error, m/s
580	$3.00 \cdot 10^{-10}$	$0.1 \cdot 10^{-10}$
600	$3.83 \cdot 10^{-10}$	$0.5 \cdot 10^{-10}$
630	$9.46 \cdot 10^{-10}$	–
650	$1.88 \cdot 10^{-9}$	$0.02 \cdot 10^{-9}$
690	$9.46 \cdot 10^{-9}$	$0.7 \cdot 10^{-9}$
750	$2.4 \cdot 10^{-8}$	–

second group of new phase particles present in the system. Their number density, N_o, depends on the nucleation and growth rates and cooling conditions. These athermal crystals are capable of deterministic growth at T_n and, moreover, a part of them having sizes $R > R_d^*$ can be developed to larger sizes already directly at T_d without any preliminary heat treatment. The number density of the latter group of clusters is given by a non-zero value of $N_V^d(t = 0)$. In the case of existence of such group of crystallites, the $N_V^d(t)$-curve should show a behavior as indicated in Fig. 1 by a full line.

An analysis of the experimental data on NaF crystal nucleation indicates that the value of $N_V^d(t = 0)$ is very low (see e.g. Fig. 1) and can be neglected. By this reason we will suppose here further on that the *second group* includes only the pre-existing crystals with sizes larger than R_n^* and smaller than R_d^*. Being supercritical, these crystals can grow up to the critical size R_d^* during heat treatment at T_n and can then be developed at T_d contributing in such a way to the experimental $N_V^d(t)$-curve. The "life time" interval of such contribution depends mainly on the difference between R_n^* and R_d^* and the crystal growth rate at T_n. The influence of the *second group* of crystals on the $N_V^d(t)$-curve begins and ends when the largest and smallest crystals from the pre-existing population exceed the value of R_d^*.

The crystals of the *first group* (crystals nucleated at T_n) before their development must move in size space from monomers to R_d^*, whereas for the pre-existing crystals (*second group*), only from size R ($R_n^* < R < R_d^*$). Hence the *second group* reaches R_d^* earlier than the former and, thus, determines the beginning of the $N_V^d(t)$-curve. As we already noted above, the effect of pre-existing crystals ceases when the smallest crystals (crystals with size close to R_n^*) from this population reach a size R_d^*. This event results in some peculiarity on the $N_V^d(t)$-curve. In other words, beginning at this moment, the $N_V^d(t)$-curve is determined only by the nucleation process at T_n. In our case the inflection in the $N_V^d(t)$-curve is attributed to the finishing of the pre-existing crystal population (see e.g. Fig. 1).

It should be noted that the number of crystals of the second group ("athermal" crystals), N_o, formed during glass preparation, is a poorly controlled quantity. By this reason, in order to eliminate this

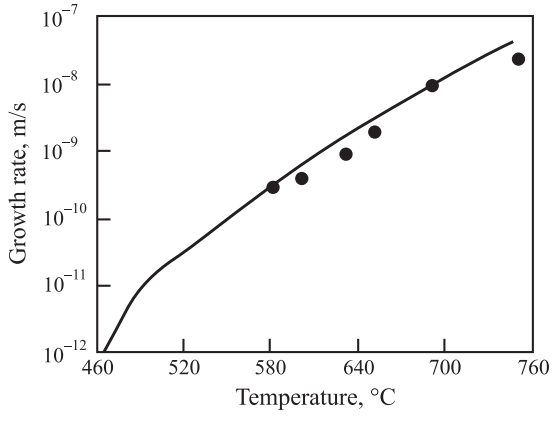

Fig. 4. Growth rates of NaF crystals versus temperature. The solid line is plotted by Eq. (10).

uncertainty special preliminary heat treatments at given temperatures in a period of time enough for establishment of the steady-state crystal size distribution were performed for a $Li_2O \cdot 2SiO_2$ glass [14]. The experimental data obtained in [14] on the nucleation kinetics in the preliminary stabilized glasses were subjected to a theoretical analysis and confirmed by simulation experiment [15–17]. Hence the "athermal" nuclei affect is the partial case of a general problem of the influence of starting conditions on the transient nucleation kinetics (see e.g. [18,19]).

In order to avoid any such effects in the present study we fitted only the advanced parts of $N_V^d(t)$-curves to Eq. (6) to estimate the steady-state nucleation rates, I_{st}, and the time-lags for nucleation, τ, as fitting parameters, since this part is determined solely by the nucleation process at T_n. The proximity between the critical sizes at T_n and T_d makes it possible at a first approximation to neglect the time t_o.

Fig. 5 shows the steady-state nucleation rates and the nucleation time-lags as functions of temperature estimated as fit parameters from the set of experimentally determined $N_V^d(t)$-curves into Eq. (6). For a self-consistent description of the experimental data concerning $I_{st}(T)$, $\tau(T)$, and $U(T)$ in the framework of the classical nucleation theory (CNT), we used further the following equations:

$$I_{st}(T) = x\frac{D(T)}{a^4}\sqrt{\frac{\sigma(T)}{k_B T}}\exp(-W^*/k_B T), \tag{7}$$

$$W^* = \frac{16\pi}{3}\frac{a^6\sigma^3(T)}{\Delta\mu^2(T)}, \tag{8}$$

$$\tau(T) = \frac{2\cdot 16}{3}\frac{a^4 k_B T\sigma(T)}{\Delta\mu^2(T)D(T)}, \tag{9}$$

$$U(T) = \frac{D(T)}{a}\left(1-\exp\left(-\frac{\Delta\mu(T)}{k_B T}\right)\right), \tag{10}$$

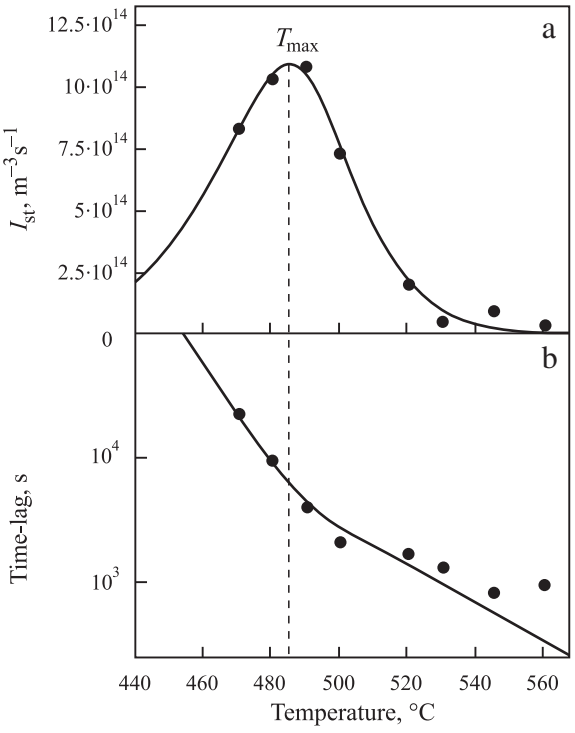

Fig. 5. Steady-state nucleation rates of NaF crystals (a) and corresponding time-lags (b) versus temperature. The solid lines result from calculations by (a) Eq. (7) and (b) Eq. (9).

where D is the effective diffusion coefficient determining both the rates of aggregation in nucleation and crystal growth, σ is the specific interfacial free energy of the critical nuclei, x is the molar fraction of precipitated component (in the present case NaF), W^* is the thermodynamic barrier for nucleation, $\Delta\mu$ is the difference between the chemical potentials of "structural" units with a size a in the super-cooled liquid and in the crystalline phase – i.e. the thermodynamic driving force for crystallization ($\Delta\mu = a^3\Delta G_V$), k_B and T are the Boltzmann constant and the absolute temperature, respectively.

To employ the above equations one needs to know the value of $\Delta\mu$ for NaF crystallization. Here $\Delta\mu$ was determined by the supersaturation relative to the equilibrium concentration C^{eq} of NaF in the undercooled melt of PTR glass. In our previous work [3], C^{eq} was estimated as a function of temperature T. We fitted the experimental data for the equilibrium solubility $C^{eq}(T)$ by the Schroeder–van Laar equation [20]

$$C^{eq}(T) = C_0\exp\left(-\frac{\Delta H_m}{RT}\frac{T_m - T}{T_m}\right), \tag{11}$$

where T_m and ΔH_m are melting point and melting enthalpy of dissolved matter (in our case NaF crystals), respectively. In the above equation, it is assumed that ΔH_m is independent of temperature. In the case of the ideal solutions C_0 is equal to 1.

Fig. 6 shows the experimental (points) dependence of C^{eq} on T taken from Ref. [3]. The solid line is plotted by Eq. (11) with $C_0 =$ 10.905 mol% estimated as fit parameter and $T_m = 1269$ K and $\Delta H_m =$ $33.35 \cdot 10^3$ J/mol taken from Ref. [21] and Ref. [22] respectively. The difference of C_0 from one shows that the solution of NaF in PTR melt is a nonideal solution.

Knowing the concentration C of the dissolved substance (NaF) and its equilibrium concentration C^{eq}, the thermodynamic driving force $\Delta\mu$ for crystallization can be evaluated as

$$\Delta\mu(T) = k_B T\ln\left(\frac{C}{C^{eq}(T)}\right). \tag{12}$$

Diffusivity, D, specific surface energy, σ, and thermodynamic driving force, $\Delta\mu$, determine the crystallization kinetics (see Eqs. (7)–(10)). Thus, we varied the temperature dependencies of $D(T)$ and $\sigma(T)$ at given values of $\Delta\mu$ (Eq. (12)) to arrive at the best agreement between calculated and experimental values of $I_{st}(T)$, $\tau(T)$, and $U(T)$. Hereby the effective diffusion coefficients for nucleation and growth are assumed to be the same. The size parameter a was considered as a fitting parameter too, estimated as 4.5 Å. It should be noted that this

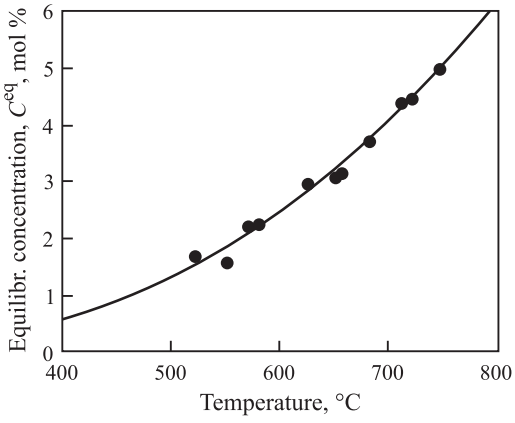

Fig. 6. Equilibrium content of NaF (mol%) in PTR glass as a function of temperature. The solid line is plotted by Eq. (11) with proper parameters.

value is very close to the cell parameter of NaF (4.6 Å). The fitting procedure deals simultaneously with the set of all experimental data, but is facilitated by the fact that the influence of $\Delta\mu$ is stronger on I_{st} than on τ and U, whereas D affects more τ and U.

The following fitting equations were used for σ (J/m^2) and D (m^2/s):

$$\sigma(T) = \sigma_0[1-\alpha(T-T_{max})], \tag{13}$$

$$D(T) = D_1(T)\cdot f_k\left(\frac{T_k-T}{\delta T}\right) + D_2(T)\cdot f_k\left(\frac{T-T_k}{\delta T}\right), \quad T_k = 773K, \tag{14}$$

where

$$\sigma_0 = 0.0735\ \mathrm{J/m^2},\ \ T_{max} = 758.4\ \mathrm{K},\ \ \alpha = 1.0162\cdot 10^{-3}\ \mathrm{K^{-1}},$$

$$D_1(T) = 1.116\cdot 10^{14}\exp\left(-\frac{51\cdot 10^4}{RT}\right),$$

$$D_2(T) = 2.468\cdot 10^{-2}\exp\left(-\frac{29.10^4}{RT}\right),$$

$$f_k(x) = \frac{1}{2}[1+\tanh(x)].$$

The above equations need a few comments. $T_{max} = 758.4$ K in Eq. (13) is the temperature of maximum nucleation rate (see Fig. 5a). In such way we fixed the value of $\sigma(T_{max}) = \sigma_0$ that together with the other parameters yields the correct maximum value of the steady-state nucleation rate. The temperature dependence of the interfacial free energy is shown in Fig. 7. To describe the temperature dependence of the nucleation time-lags and also to achieve the correct value of $U(T)$, a combination of two diffusion coefficients corresponding to low (D_1) and high (D_2) temperatures was employed (see Fig. 8). The transition from D_1 to D_2 was performed via a function f_k. δT and T_k are the width of this transition and its average temperature, respectively.

5. Discussion

Since the PTR glass contains only 5 mol% NaF, the formation of NaF crystals results in a strong depletion in F of the residual melt, and when the NaF content in the melt reaches equilibrium, the very early stage of coarsening begins [12]. However, in our case, we did not achieve a detectable coarsening stage due to insufficient experimental time. The evolution of the residual melt composition and related phenomena were investigated in detail in some of our previous papers [2–5]. The saturation of the crystal size versus time plot (Fig. 3) reflects the attainment of equilibrium between the NaF crystals and the residual

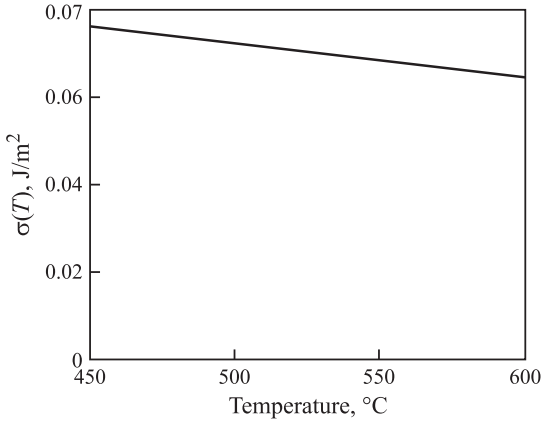

Fig. 7. Specific free energy of the interface critical nucleus/liquid versus temperature. The line is plotted by Eq. (13).

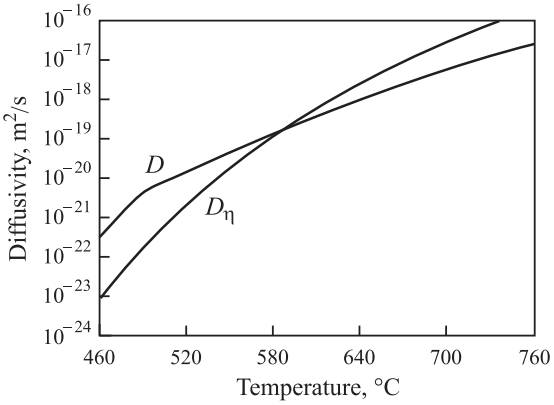

Fig. 8. Effective diffusion coefficient, D, estimated from crystallization kinetics and D_η estimated from viscosity data via the Stokes–Einstein–Eyring equation.

melt. As we noted earlier, to obtain the temperature dependence of the crystal growth rates we used only the initial part of the $R(t)$ time plots, such as that shown in Fig. 3, since in the early stages of the phase transformation crystal growth is determined by a time-independent effective diffusion coefficient. The change of the residual melt composition can be also neglected for the analysis of the nucleation kinetics due to the extremely small nuclei sizes and hence very small volume fraction of crystalline phase.

The fitting procedure described in Section 4 is complex because it simultaneously includes all parameters governing the overall crystallization kinetics (the steady-state nucleation rates, the time-lags for nucleation, and the crystal growth rates) measured in a wide temperature interval covering about 300 °C — from 470 °C to 750 °C. The fitting parameters (the surface free energy and the effective diffusion coefficient) shown in Figs. 7 and 8 as a function of temperature, respectively, together with the thermodynamic driving force give a very reasonable description of the experimental data (please compare the experimental points and calculated lines in Figs. 4 and 5). The self-consistent description of both nucleation and growth kinetics using the same temperature dependencies of $\sigma(T)$ and $D(T)$ gives indirect evidence for its validity. Therefore the following comments on the above dependencies can be made.

The specific surface energy, σ, estimated via the experimental nucleation rates in the framework of CNT for silicate glasses and metallic glasses, as a rule, increases with temperature (see e.g. [23]). It should be stressed that, as opposed to PTR glass, in these cases the crystal composition is equal or close to that of liquid. For PTR glass, however, σ weakly *decreases* with increasing temperature (Fig. 7). Finally, together with a decreasing thermodynamic driving force this results in an increase of the thermodynamic barrier shown in Fig. 9. The latter result is consistent with the predictions of the CNT.

The value of σ estimated via nucleation rates relates to the nuclei with critical or near critical size. Thus, the evolution of σ shown in Fig. 7 is the combination of the pure temperature dependence and the size dependence resulting from the increase of critical size with temperature shown in Fig. 9. This size dependence can be, in principle, incorporated into Eqs. (7)–(9), e.g. as was done in Ref. [21]. However, despite its long history, the problem of a size dependent specific interfacial free energy remains open [24–27].

The temperature dependence of the effective diffusion coefficient that governs both nucleation and growth kinetics is shown in Fig. 8. Its activation enthalpy decreases with temperature. Such behavior is common for temperature activated processes. It should be noted that the experimental data for the nucleation time-lag relates to the temperature interval that includes both D_1 (low temperatures) and D_2 (high temperatures), whereas the U measurements were performed only at temperatures corresponding to D_2. Therefore, to complete the analysis of the effective diffusivity (Fig. 8), we estimated the diffusion

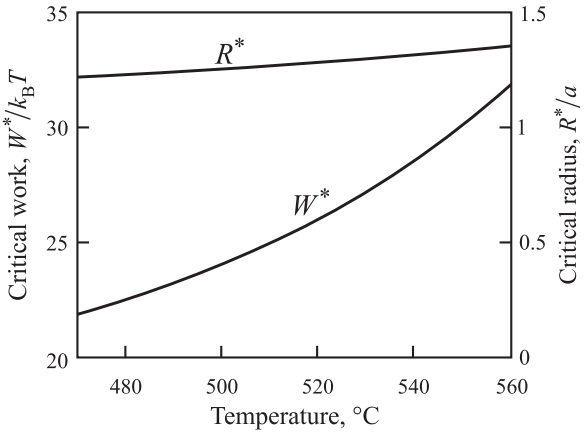

Fig. 9. Thermodynamic barrier for nucleation, W^*, and critical size, R^*, versus temperature.

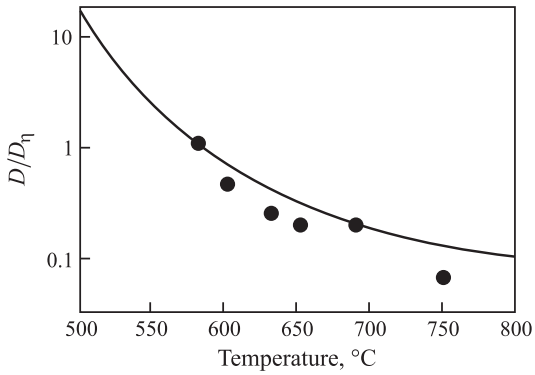

Fig. 10. The ratio of D to D_η versus temperature.

coefficient in an independent way by the Stokes–Einstein–Eyring equation

$$D_\eta = k_B T/a\eta, \tag{15}$$

using viscosity data available for PTR glass [28] that are described by the following Vogel–Fulcher–Tammann equation:

$$\log\eta = -2.40 + 4740/(T-416), \tag{16}$$

where the viscosity and temperature are given in Pa·s and K, respectively.

The difference between D and D_η does not exceed 1.5 orders of magnitude and this is an unexpected result. The effective diffusion coefficient D estimated from NaF crystallization kinetics reflects the transport of the "building" elements involved in the formation of NaF crystals. Since the PTR glass already contains 15% Na_2O, the kinetics of NaF crystallization is limited by the fluorine mobility. Despite the deficiency of diffusion coefficient data for fluorine in silicate glasses, we expect, based on F–O interdiffusion coefficient measurements for some melts of the Na_2O–Al_2O_3–SiO_2 system [29], that D_F is 5–8 orders of magnitude *higher* than D evaluated from NaF crystallization kinetics. Here it should be recalled that the diffusion coefficient of sodium in common sodium calcium silicate glasses varies between 10^{-13} and 10^{-10} m^2/s (see e.g. [30,31]) in the temperature interval 700–800 K (the temperatures of interest here), then these values are also considerably higher than D. Thus one could suppose that the transport processes of F and Na determining crystallization kinetics are complex and may be somewhat correlated with viscous flow. For instance, "structural units" of the glass-forming melt could perhaps cooperatively move to liberate space for the NaF crystal boundary advance. Here it should be recalled that the reduction of the NaF content in PTR glass results in the strong increase of viscosity [3]. However the correlation between D and D_η decreases with decreasing temperature, as one can see from Fig. 10 (the ratio D/D_η versus temperature). This effect is known as decoupling (or breakdown) and according to Ediger et al. [32] it is expected in fragile glasses in the neighborhood of the glass transition temperature T_g. Please recall that according to Ref. [28] the fragility index for PTR glass is about 33. This means that PTR glass is positioned between the typical "strong" and "fragile" glasses.

6. Conclusions

The detailed kinetics of NaF crystallization in UV-unexposed PTR glass was experimentally studied for the first time. Steady-state nucleation rates, nucleation time-lags and crystal growth rates were estimated in a temperature interval covering almost 300 °C, from T_g ~ 470 °C up to 750 °C. A self-consistent description of these data in the framework of CNT was presented using the interfacial free energy and the effective diffusion coefficient as adjustable parameters. The diffusivities calculated from crystallization kinetics and viscous flow undergo a decoupling phenomenon already demonstrated for other fragile glasses.

Acknowledgments

We are thankful to Guilherme P. Souza and Jürn W. P. Schmelzer for valuable discussions and to the Brazilian funding agencies CNPq, grant # 2012/17417-9 and CEPID grant # 2013/07793-6, São Paulo Research Foundation (FAPESP) for generous funding of this research.

References

[1] J. Lumeau, A. Sinitskii, L. Glebova, L.B. Glebov, E.D. Zanotto, Phys. Chem. Glasses: Eur. J. Glass Sci. Technol. B 48 (2007) 281–284.
[2] G.P. Souza, V.M. Fokin, E.D. Zanotto, J. Lumeau, L. Glebova, L.B. Glebov, Phys. Chem. Glasses: Eur. J. Glass Sci. Technol. B 50 (2009) 311–320.
[3] V.M. Fokin, G.P. Souza, E.D. Zanotto, J. Lumeau, L. Glebova, L.B. Glebov, J. Am. Ceram. Soc. 93 (2010) 716–721.
[4] G.P. Souza, V.M. Fokin, C.A. Baptista, E.D. Zanotto, J. Lumeau, L. Glebova, L.B. Glebov, J. Am. Ceram. Soc. 94 (2011) 2906–2911.
[5] G.P. Souza, V.M. Fokin, C.F. Rodrigues, A.C.M. Rodrigues, E.D. Zanotto, J. Lumeau, L. Glebova, L.B. Glebov, J. Am. Ceram. Soc. 94 (2011) 86–91.
[6] G. Tammann, Z. Phys. Chem. 25 (1898) 441–479.
[7] I. Gutzow, J. Schmelzer, The Vitreous State: Thermodynamics, Structure, Rheology and Crystallization, Springer, Berlin, 1995.
[8] V.M. Fokin, E.D. Zanotto, N.S. Yuritsyn, J.W.P. Schmelzer, J. Non-Cryst. Solids 352 (2006) 2681–2714.
[9] V.M. Fokin, E.D. Zanotto, J.W.P. Schmelzer, J. Non-Cryst. Solids 278 (2000) 24–34.
[10] M.J. Davis, Glastechn. Ber. 73 (2000) 170–177, (C1).
[11] M.J. Davis, J. Am. Ceram. Soc. 84 (2001) 492–496.
[12] V.V. Slezov, Kinetics of First-order Phase Transitions, WILEY-VCH Verlag, Berlin, GmbH, 2008.
[13] F.C. Collins, Z. Electrochem. 59 (1955) 404–407;
D. Kashchiev, Surf. Sci. 14 (1969) 209.
[14] V.M. Fokin, A.M. Kalinina, V.N. Filipovich, J. Cryst. Growth 52 (1981) 115–121.
[15] Z. Kozisek, Cryst. Res. Technol. 23 (1988) 1315–1322.
[16] K.F. Kelton, A.L. Greer, Phys. Rev. B 38 (1988) 10089–10092.
[17] A.L. Greer, K.F. Kelton, J. Am. Ceram. Soc. 74 (1991) 1015–1022.
[18] D. Kashchiev, Nucleation: Basic Theory with Application, Butterworth-Heinemann, Oxford, 2000.
[19] K.F. Kelton, A.L. Greer, Nucleation in Condensed Matter, Pergamon Materials Series, vol. 15, Elsevier Ltd., 2010
[20] I. Prigogine, R. Defay, Chemical Thermodynamics, Longmans Green, London, 1953.
[21] Handbook of Chemistry and Physics, 54th edition CRC Press, 1973–1975.
[22] H. Mediaas, P. Chartrand, O. Tkatcheva, A.D. Pelton, T. Ostvold, Can. Metall. Q. 40 (2001) 13–32.
[23] V.M. Fokin, E.D. Zanotto, J. Non-Cryst. Solids 265 (2000) 105–112.
[24] J.W. Gibbs, Trans. Conn. Acad. 3 (1878) 343–524.
[25] R.C. Tolman, J. Chem. Phys. 17 (1949) 333–337.
[26] J.W.P. Schmelzer, I. Gutzow, J. Schmelzer Jr., J. Colloid Interface Sci. 178 (1996) 657–665.
[27] V.G. Baidakov, Russ. J. Phys. Chem. 86 (2013) 1–3.
[28] J. Deubener, H. Bornhöft, S. Reinsch, R. Müller, J. Lumeau, L.N. Glebova, L.B. Glebov, J. Non-Cryst. Solids 355 (2009) 126–131.
[29] D.B. Dingwell, C.M. Scarfe, Earth Planet. Sci. Lett. 73 (1985) 377–384.
[30] Sciglass_database, http://www.esm-software.com/sciglass.
[31] H. Mehrer, A.W. Imre, E. Tanguep Nijokep, J. Phys. Conf. Ser. 106 (2008) 012001.
[32] M.D. Ediger, P. Harrowell, L. Yu, J. Chem. Phys. 128 (2008) 034709.